Geological Survey
of Canada

RADIOGENIC AGE AND ISOTOPIC STUDIES: REPORT 13

Current Research
2000-F3

Microstructure of Neoarchean zircon from the Acasta gneiss complex, Northwest Territories

N. Sanborn, R. Stern, S. Desgreniers, and G.A. Botton

2000

Natural Resources Canada Ressources naturelles Canada

Canada

Contents/Contenu

Page 1 report/Début de l'article

©Her Majesty the Queen in Right of Canada, 2000
Catalogue No. M44-2000/F3E-IN
ISBN 0-660-18229-7

Available in Canada from the
Geological Survey of Canada Bookstore website at:
http://www.nrcan.gc.ca/gsc/bookstore (Toll-free: 1-888-252-4301)

A copy of this publication is also available for reference by depository libraries across Canada through access to the Depository Services Program's website at http://dsp-psd.pwgsc.gc.ca

Price subject to change without notice

All requests for permission to reproduce this work, in whole or in part, for purposes of commercial use, resale or redistribution shall be addressed to: Geoscience Information Division, Room 200, 601 Booth Street, Ottawa, Ontario K1A 0E8.

Authors' addresses

N. Sanborn *(nsanborn@nrcan.gc.ca)*
R. Stern *(rstern@nrcan.gc.ca)*
GSC Ottawa
601 Booth Street
Ottawa, Ontario K1A 0E8

S. Desgreniers *(serge@physics.uottawa.ca)*
Ottawa-Carleton Institute of Physics
University of Ottawa
150 Louis Pasteur
Ottawa, Ontario K1S 5B6

G.A. Botton *(gbotton@nrcan.gc.ca)*
Materials Technology Laboratory
CANMET, Natural Resources Canada
568 Booth St.
Ottawa, Ontario K1A 0G1

Contents/Contenu

Page 1 report/Début de l'article

Microstructure of Neoarchean zircon from the Acasta gneiss complex, Northwest Territories

N. Sanborn, R. Stern, S. Desgreniers, and G.A. Botton
Continental Geoscience Division, Ottawa

Sanborn, N., Stern, R., Desgreniers, S., and Botton, G.A., 2000: Microstructure of Neoarchean zircon from the Acasta gneiss complex, Northwest Territories; Geological Survey of Canada, Current Research 2000-F3; Radiogenic Age and Isotopic Studies: Report 13, 12 p. (CD-ROM).

Abstract: The microstructure of zircon from a late Archean granite dyke from the Acasta gneiss complex was investigated using a number of microprobe techniques. Zircons from the study sample are composed of low-Ca, unaltered and high-Ca, altered domains. Transmission electron microscopy indicates that the unaltered areas have a distorted crystalline microstructure. The detailed microstructure of altered zircon is heterogeneous, composed of a mixture of low-Ca, crystalline domains and amorphous, high-Ca domains. Calculations show that radiation damage accumulated from the decay of U and Th over the entire life of the sample would have rendered the sample metamict. We conclude that the observed crystalline structure is the result of recrystallization late in the geological history of the sample. Sensitive high-resolution ion microprobe U-Pb ages from the low Ca, crystalline zircon are concordant, suggesting that Pb loss did not accompany the recrystallization process.

Résumé : Au moyen de techniques de microsondage, on analysé la microstructure du zircon contenu dans un dyke de granite de l'Archéen tardif provenant du complexe gneissique d'Acasta. Les zircons de l'échantillon à l'étude sont composés de domaines inaltérés à faible teneur en Ca et de domaines altérés à haute teneur en Ca. La microscopie électronique à transmission révèle que les zones inaltérées ont une microstructure cristalline déformée. La microstructure détaillé du zircon altéré est hétérogène et comporte un mélange de domaines cristallins à faible teneur en Ca et de domaines amorphes à haute teneur en Ca. D'après les calculs, le dommage causé par le rayonnement dû à la décomposition de U et de Th pendant toute la durée de vie de l'échantillon aurait transformé l'échantillon en métamicte. Les chercheurs concluent que la structure cristalline observée est le résultat d'une recristallisation tard dans l'histoire géologique de l'échantillon. Les datations U-Pb au moyen de la microsonde ionique à haute résolution et à haut niveau de sensibilité d'un zircon cristallin à faible teneur en Ca concordent, laissant supposer qu'il n'y a pas eu de perte de Pb durant le processus de recristallisation.

INTRODUCTION

Zircon ($ZrSiO_4$) is a common accessory mineral found in a variety of igneous, metamorphic, and sedimentary rocks and is one of the most widely used minerals in geochronological studies. During crystallization, zircon incorporates U and Th into its crystal lattice, and the decay of U and Th to Pb provides several robust chronometers. However, the U-Th-Pb systematics are subject to disturbance, most commonly the loss of radiogenic Pb. The correlation between the concentration of radioactive elements and discordant isotopic systematics suggests that metamictization (crystal lattice damage caused by the decay of the radioactive element) facilitates the loss of radiogenic Pb (Silver and Deutsch, 1963). Metamictization is caused largely by nucleic recoil of U and Th during alpha decay. The bombardment of the crystal lattice by large nuclei progressively distorts and eventually destroys the crystal lattice (Holland and Gottfried, 1955; Chakoumakos et al., 1987; Murakami et al., 1991). Although the cause of metamictization is believed to be well constrained, the nature of metamict zircon has been the subject of debate. Early workers suggested that the structure of metamict zircon consisted of off-axis zircon crystallites (Bursill and McLaren, 1966), or a mixture of SiO_2 and ZrO_2 (Wasilewski et al., 1973). However, Farges and Calas (1991) have shown that results of X-ray diffraction and transmission electron microscopy studies are not consistent with either of these models. A structure composed of mixed crystalline and amorphous microdomains 1 to 10 nm in size (Chakoumakos et al., 1987) or amorphous $ZrSiO_4$ (Holland and Gottfried, 1955) is more compatible with available data.

The purpose of this study is to characterize the structure of complex, high-uranium, Neoarchean zircon from the Acasta gneiss complex, Northwest Territories. The high spatial resolution of Raman spectroscopy and transmission electron microscopy, combined with detailed age, U, and Th data from sensitive high-resolution ion microprobe (SHRIMP) analyses, allow us to characterize the microstructure of two different zircon features found in individual grains. Zircons from the study sample have been extensively altered and we believe that the chemical alteration is largely responsible for the observed Pb loss. With this study, we hope to clarify the role of microstructure in zircon alteration and Pb-loss processes.

SAMPLE INVESTIGATED

The rock sample chosen for study is a late Archean granite dyke from the Acasta gneiss complex in the Northwest Territories. The Acasta gneiss complex comprises basement rocks in the westernmost Slave Province. It is composed of polydeformed, metamorphosed, and migmatitic amphibolite-tonalite-granite gneiss and contains the oldest known terrestrial rocks (Stern and Bleeker, 1998; Bowring et al, 1989). The oldest gneiss units are cut by several generations of pegmatite and granite dykes.

The study sample, BNB-95-110c, was collected from one of these granite dykes. The dyke is roughly 30 cm wide and the contacts are parallel with the foliation in the host rock. It is weakly deformed, with planar fabric parallel to the foliation in the host rock (Fig. 1). The dyke is visibly altered at outcrop scale with feldspar taking on a reddish tint. Petrographic studies provide further evidence of alteration. Virtually all feldspar has been sericitized and carbonate and epidote are present along cracks and grain boundaries. Zircons separated from sample 110c are prismatic with an aspect ratio of 2:1 to 3:1; they are light to dark brown, with well formed to curvilinear facets. Their outer surfaces are generally pitted. Most grains have a euhedral external morphology, although the margins of some grains are embayed, which suggests a minor degree of dissolution and reprecipitation. Clarity varies from moderately turbid to opaque depending on magnetic susceptibility, and most grains contain numerous inclusions and fractures. Areas of greater clarity and lighter colour are preserved within many individual grains.

Internal features

The internal features of the zircons were documented in back-scattered electron and cathodoluminescence imaging modes using a Cambridge Instruments S360 scanning electron microscope at the Geological Survey of Canada. Due to

Figure 1. *Outcrop of granite dyke (sample BNB-95-110c). The sample was collected from the light-coloured granite sheet in the centre of the photo. Note sledge hammer for scale.*

Contents/Contenu

Page 1 report/Début de l'article

low-intensity cathodoluminescence emission, we were unable to resolve any internal structures using this method. Cathodoluminescence emission is commonly attenuated in samples with significant crystal lattice damage. Internal structures were resolved more effectively using back-scattered electron images, where varying degrees of brightness are controlled by variations in average atomic number. The majority of the zircons contain variably dark and bright patches in these images (Fig. 2). The dark patches are irregularly shaped and commonly preserve primary oscillatory zoning; their margins commonly truncate any zoning. Electron microprobe compositional maps and spot analyses document an enrichment in Ca in these dark patches relative to the bright areas. SHRIMP analyses of these patches also reveal concentrations of common Pb of over 50 ppb. The addition of Ca and excess Pb to this type of zircon suggests some form of chemical alteration of the zircon showing dark characteristics in back-scattered electron images. Therefore, in this study, these dark patches will be referred to as 'altered zircon'.

An exceptionally dark rim roughly 3 μm thick commonly defines the boundary between bright and dark zircon. The contact between the rim and the bright zircon is sharp, whereas the transition from rim to dark (altered) zircon is gradational. The appearance of this rim is suggestive of a reaction front migrating through the zircon (e.g. Fig. 2b).

Bright patches may be completely enclosed by the darker zircon and are normally preserved in the interior of the grains. SHRIMP analyses from the bright patches generally yield concordant U-Pb ages, and have a mean age of 2875 Ma (Sanborn, 2000; R. Stern and N. Sanborn, unpub. data, 1999). Brief exposure to HF vapour is sufficient to enhance the visibility of oscillatory zoning in the bright zircon domains in the back-scattered electron images (Fig. 2). However, some of the bright zircon is weakly zoned, which might be the result of incomplete recrystallization (Pidgeon, 1992). The bright zircon domains contain little to no Ca or common Pb and therefore are referred to as 'unaltered zircon'.

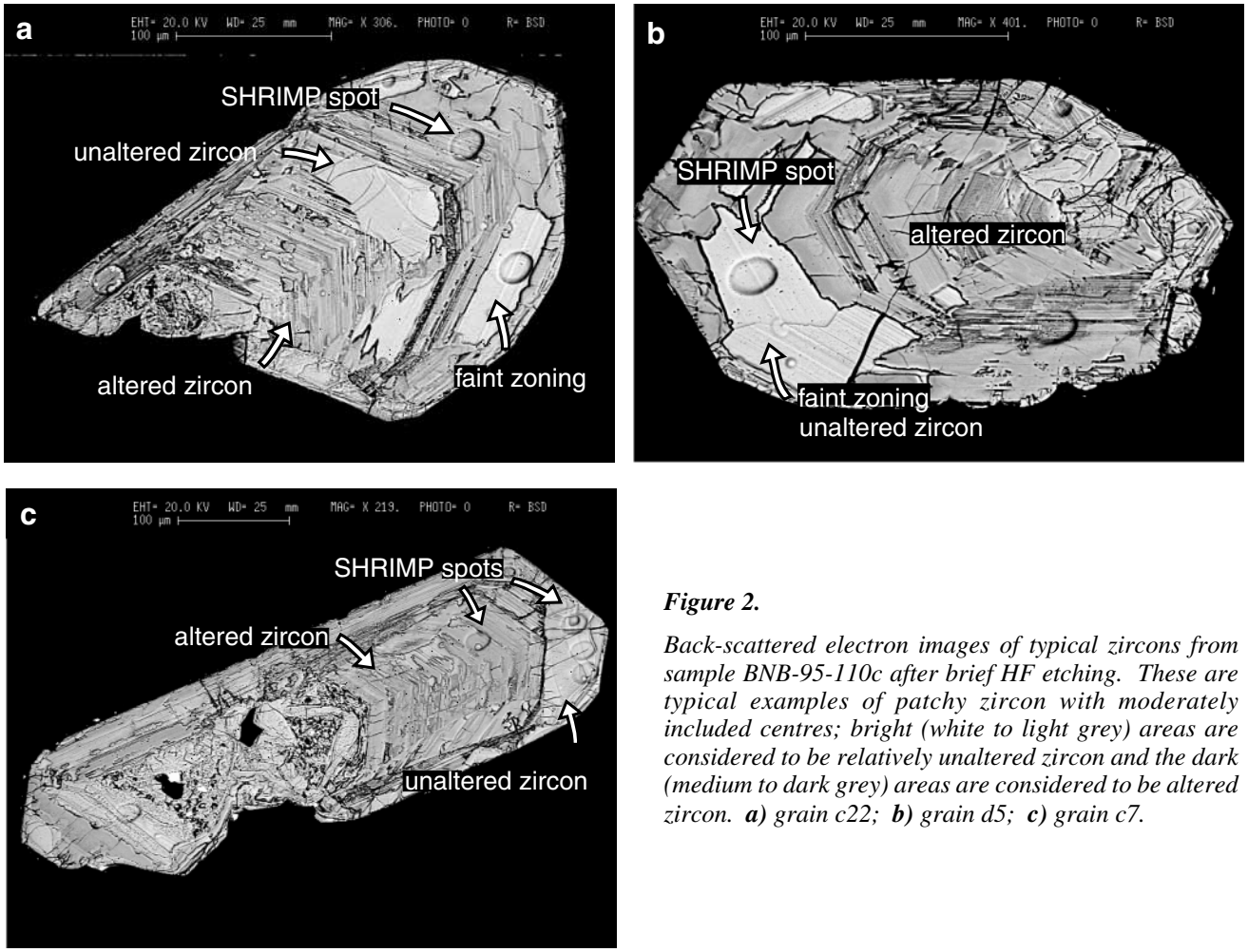

Figure 2.

Back-scattered electron images of typical zircons from sample BNB-95-110c after brief HF etching. These are typical examples of patchy zircon with moderately included centres; bright (white to light grey) areas are considered to be relatively unaltered zircon and the dark (medium to dark grey) areas are considered to be altered zircon. ***a)*** *grain c22;* ***b)*** *grain d5;* ***c)*** *grain c7.*

METHODS

Raman microprobe

The Raman microprobe is a vibrational spectroscopic tool used primarily by geologists in the identification of mineral and fluid inclusions. However, recent work by Nasdala et al. (1995, 1996, 1998) and Wopenka et al. (1996) has shown its usefulness in quantifying the degree of metamictization of zircon. A typical Raman apparatus consists of a laser source, the sample, and a high stray-light rejection spectrometer. Intense monochromatic light from the laser is focused through a series of lenses or mirrors onto the sample. Although most of the light is transmitted through a non-opaque sample, a small part of it is scattered. Most of the scattered light maintains the same wavelength as the incident light, known as 'Rayleigh scattered light'. However, a small component is scattered at a wavelength slightly higher or lower than that of the incident light. The change in wavelength of scattered light is known as the 'Raman effect' and is illustrated in Figure 3. The scattered light is collected and its wavelength and intensity recorded by the spectrometer. The data are presented as a plot of relative change in wave numbers (the difference between the reciprocals of wavelengths of Rayleigh and Raman scattered light) against intensity.

The basis of the Raman effect can be explained using simple energy diagrams (Fig. 4). The vibrations of atoms within the crystal lattice of a mineral are quantized. The quantum of vibrational energy is known as a 'phonon'. As light interacts with the vibrations of the crystal lattice, some of the energy from the photon may be transferred to one of the phonons, exciting the system to a higher vibrational state. The photon is therefore scattered at a lower frequency (higher wavelength=lower wave number) having lost some of its energy to the vibrational excitation. The reverse process is also possible, where an excited vibrational state transfers a phonon to the incoming photon and the scattered light is thus more energetic (lower wavelength=higher wave number).

The Raman spectrum of each mineral is distinct, although the pattern is subject to modification. With increased metamictization, two changes occur, a shift of peak positions to lower wave numbers and a systematic peak broadening (Nasdala et al., 1995). The first effect can be explained by the lengthening of interatomic bonds during metamictization. Longer bonds vibrate at a lower frequency, and consequently the scattered light is shifted to lower wave numbers. The second effect is the result of the distortion of the crystal lattice during metamictization. A distorted crystal lattice no longer has a unique frequency of vibration, which varies with the degree of distortion. Light interacting with phonons of slightly varied frequencies will be scattered correspondingly and the result is a broadened peak. Complete metamictization leads to a loss of long-range atomic ordering characterized by an ill-defined vibrational spectrum.

Raman spectroscopy is a nondestructive technique. Consequently, subsequent ion-probe analyses are unaffected by the Raman analysis (Nasdala et al., 1998). This makes it an excellent method to use to pre-screen samples before geochronological study. By assessing the degree of crystallinity, only the most robust portions of zircon can then be selected for analysis.

Sample preparation for Raman analysis is very simple — the style of epoxy mounts used for SHRIMP work (described *in* Stern, 1997) is adequate. Because fluorescence from the sample or the epoxy can mask the Raman signal, zircon mount IP102 was made specifically for the Raman analysis using Epo-tek 301®, a low-fluorescing epoxy. The Raman work was carried out at the High Pressure Physics Laboratory at the Physics Department of the University of Ottawa. MicroRaman spectra were recorded on a Jobin-Yvon S3000 subtractive triple spectrometer equipped with a liquid-nitrogen-cooled charge coupled device detector. Samples at room temperature were excited with the 514.53 nm line of the Ar+ laser at a power less than 200 mW at the source, in a nearly 180° scattering geometry using an Olympus 50X microscope objective. The volume analyzed is a spot 15 to

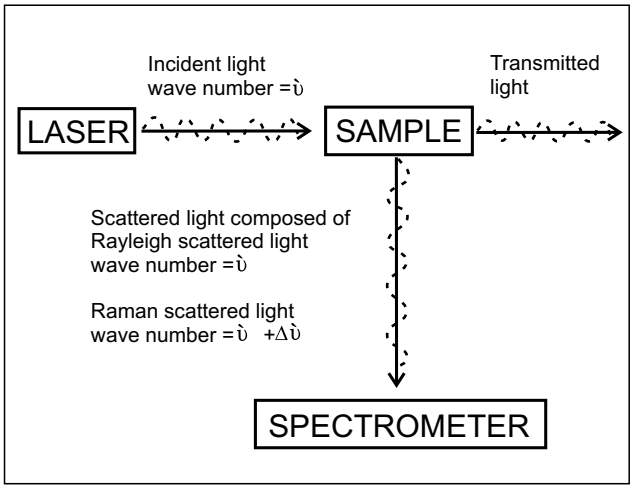

Figure 3. *Schematic of a typical Raman experiment (*after *Roberts and Beattie, 1995).* See *text for further explanation.*

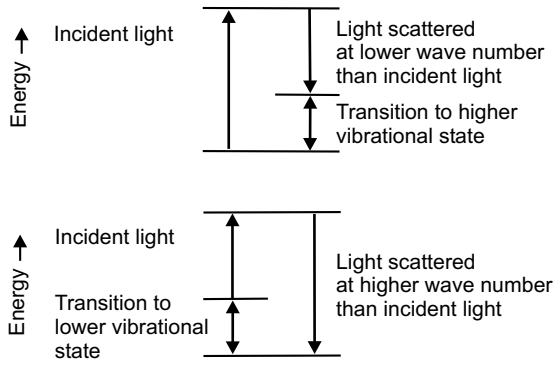

Figure 4. *Simple energy diagrams illustrating the origin of the Raman effect (*after *Roberts and Beattie, 1995).* See *text for further explanation.*

Contents/Contenu
Page 1 report/Début de l'article

20 µm in diameter and 100 µm deep. A field aperture was also used to reduce the depth of field and consequently to enhance the Raman signal-to-background ratio. The instrumental spectral line width was kept smaller than 4 cm^{-1}. Following Nasdala et al. (1996, 1998), the degree of metamictization is estimated from the full width at half the maximum intensity of the Raman peak at 1000 cm^{-1}, which is measured using an in-house line profile analysis program (Desgreniers and Lagarec, 1994). A Lorentzian curve is fitted to the data and the measured peak width, also known as 'bandwidth' (b_s), is derived from the equation of the curve. An additional calculation is needed to determine the true bandwidth (b). True bandwidths do not correlate directly with b_s and are strongly influenced by instrumental conditions. The conversion to true bandwidth is necessary to quantify more rigourously the degree of metamictization; true bandwidths are calculated from the measured bandwidth and the spectral resolution of the instrument (s) using the following equation of Irmer (1985):

$$b = b_s \sqrt{1 - 2(s/b)^2}$$

Transmission electron microscopy

Thin membranes of zircon, appropriate for transmission electron microscopy (TEM) studies, were prepared by Rob Patterson at Fibics Inc., Ottawa, using the 'lift-out' technique described below. Two zircon grains were selected for analysis, grain D23 on SHRIMP mount IP82 and grain TEM 11 on a mount made specifically for TEM analysis. SHRIMP analysis on a large, bright patch of grain D23 yielded a concordant U-Pb age and detected only trace amounts of common Pb. Both these properties are typical of unaltered zircon from this sample. Using the back-scattered electron image of grain D23 as a guide, an area composed of an unaltered zone, a very dark transition zone, and an adjacent altered patch was selected for TEM study. An area composed solely of altered zircon was selected from grain TEM 11. Using a Micrion 2500 focused ion beam instrument, a Ga^+ ion beam, with an accelerating voltage of 50 kV, was used to excavate two adjacent trenches, roughly 15 µm long and 10 µm deep, leaving a thin, vertical slice of zircon between them. The slice of zircon is a cross-section through the selected area. This vertical slice was further thinned to a thickness of roughly 80 nm using the focused ion beam. After thinning was completed, the Ga^+ ion beam was used to cut through the edges and bottom of the membrane to free it from the grain. The electrostatic charge on the tip of a very fine needle was used to transfer the membrane onto a copper grid for analysis. The microscope used was a Philips CM20FEG operated at 200 keV, located at the Materials Technology Laboratory, CANMET, Ottawa. The system is equipped with a field-emission gun making it possible to obtain electron probe sizes in the order of 1 to 2 nm. An energy-dispersive X-ray detector and a scanning unit are also available on the microscope so that elemental maps at high spatial resolution (with 1–2 nm probe sizes) and scanning annular dark field images can be obtained.

RESULTS

Raman results

As a zircon becomes metamict, the long-range order of the crystal structure is lost and the width of vibrational bands increases (Nasdala et al., 1995). Stacked spectra of two variably crystalline zircons are used to illustrate this effect (Fig. 5 and Table 1). The upper spectrum corresponds to Archean sample FG2, from the Abitibi Subprovince in Quebec (Mortensen, 1993), and the lower spectrum is from the Mud Tank zircon, an early Proterozoic, gem-quality zircon from Australia (Black and Gulson, 1978). The band at roughly 1000 cm^{-1} is characteristic of zircon, and this vibrational mode (SiO_4 asymmetrical stretch) is most affected by metamictization (Nasdala et al., 1995). Raman data are presented in Table 1. The measured full width at half the maximum intensity of the 1000 cm^{-1} band of the Mud Tank zircon is 2.5 cm^{-1}. In cases such as this, where the measured bandwidth (2.5 cm^{-1}) is comparable to or less than

Table 1. Structural data for crystalline test zircons

Sample	Raman bandwidth (cm^{-1})	Radiation dose (alpha-events/mg)
Mud Tank	2.5*	0.01 x 10^{16}
FG2	5*–8.5**	0.09 x 10^{16}

* b_s < or ≅ s; therefore true bandwidth b is not given (Irmer; 1985)
** b_s >> s; therefore true bandwidth b is given (Irmer, 1985)

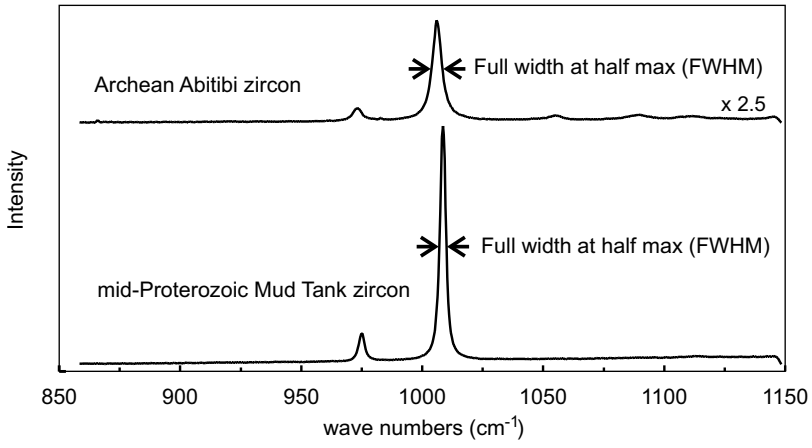

Figure 5.

Comparison of the Raman peak at 1000 cm^{-1} for variably crystalline zircons. The lower spectrum is that of a low-U, highly crystalline, early Proterozoic zircon. The upper spectrum is that of a moderately metamict, Archean zircon. Note that the spectrum of the more crystalline zircon is roughly half as broad and much more intense than that of the metamict zircon.

Table 2. Comparison of radiation dose and Raman bandwidths for a given degree of crystallinity.

Degree of crystallinity*	Raman bandwidth*	Dose** (alpha events/mg)	Diffraction Pattern**
very well crystallized to well crystallized	1–5 cm^{-1} 5–10 cm^{-1}	Stage I less than 0.3×10^{16}	sharp, pinpoint diffraction spots
intermediate to metamict	10–20 cm^{-1} 20–30 cm^{-1}	Stage II 0.3×10^{16} to 0.8×10^{16}	diffuse, elliptical diffraction spots
highly metamic (complete amorphization)	greater than 30 cm^{-1}	Stage III greater than 0.8×10^{16}	diffuse halos
*Nasdala et al. (1998) **Murakami et al. (1991)			

the spectral slit width (4 cm^{-1}), the half width is measured with great uncertainty even after mathematical correction. Despite the uncertainty in the calculation of the exact bandwidth, the scheme outlined by Nasdala et al. (1998) as shown in Table 2 suggests that this bandwidth corresponds to the structure of a very well crystallized zircon.

The true full width at half the maximum intensity of the 1000 cm^{-1} band for the sample FG2 is 5 to 8.5 cm^{-1} depending on the U content of the area selected for analysis. According to the scheme presented in Nasdala et al. (1998), this bandwidth is consistent with a well crystallized zircon. However, the wider bandwidth suggests a more damaged structure, which is consistent with the greater age and U content of sample FG2.

The radiation dose is calculated as the number of alpha-events that occurred for each milligram of sample. Dose calculations are another means of predicting the extent of structural damage in a crystal. The calculation, as given in Holland and Gottfried (1955), factors in the age and the U and Th concentrations of the sample. The net radiation dose for the Mud Tank zircon is calculated to be 0.01×10^{16} alpha-events/mg, using an age of 732 Ma and average U and Th concentrations (Black and Gulson, 1978). Murakami et al. (1991) compared radiation dosages to TEM diffraction patterns and outlined three stages of zircon structure, from highly crystalline to completely amorphous, and defined each stage by a range of radiation doses. According to that scheme, the dose received by the Mud Tank zircon is consistent with a highly crystalline zircon. The average net radiation dose estimated for sample FG2 using this method is 0.09×10^{16} alpha-events/mg. This dose is also consistent with well crystallized zircon according to the stages of metamictization outlined by Murakami et al. (1991).

Raman spectra for BNB-95-110c zircons were obtained for both bright, unaltered and dark, altered patches from single grains. The results for three grains, d5, c7 and c22, which are representative of all zircons analyzed, are presented as spectra with identical vertical and horizontal scales for comparison (Fig. 6). The back-scattered electron images for these grains are found in Figure 2. Figure 6a shows the Raman spectra for the unaltered portions of three different zircon grains. In each case, a large, bright patch, similar to those that yield concordant U-Pb ages, was selected for analysis. Care was taken to ensure that there was no overlap with adjacent dark patches. The characteristic band at ~1000 cm^{-1} was not observed for any of the bright zircon, suggesting a complete loss of crystallinity.

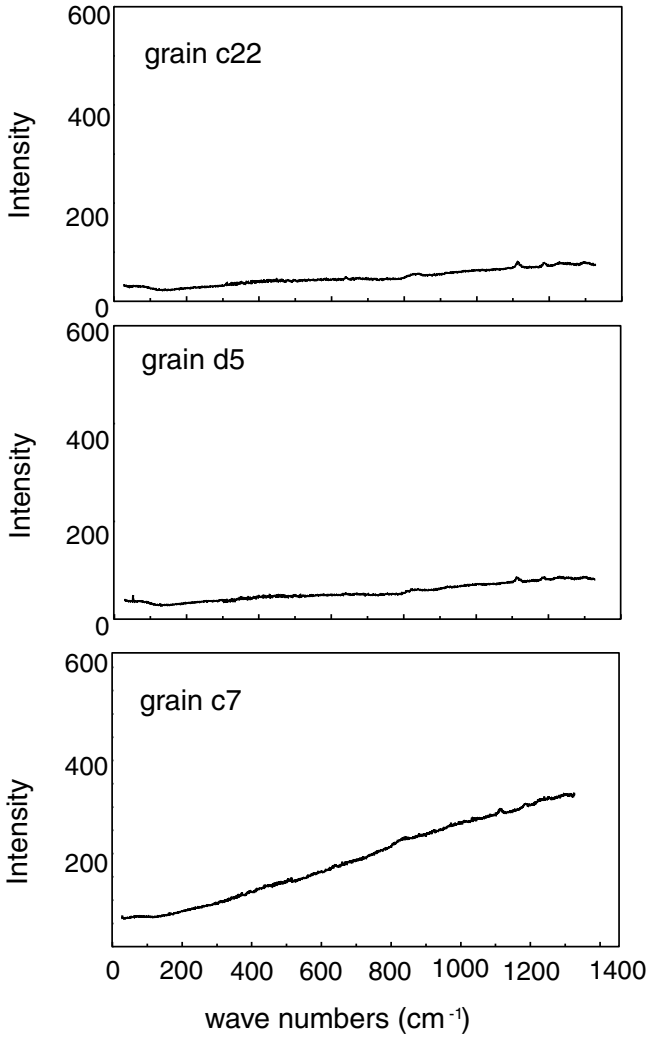

Figure 6. a) *Raman spectra of the unaltered domains (bright in back-scattered electron images) of three typical zircons from sample 110c. There is no indication of the SiO_4 stretching peak at roughly 1000 cm^{-1}, which suggests that the analyzed parts of the zircons are completely metamict.*

Contents/Contenu
Page 1 report/Début de l'article

Raman spectra for the dark, altered areas adjacent to the bright patches of the same three grains are presented in Figure 6b. As in the unaltered zircon, there is no band at 1000 cm^{-1}, again suggesting complete metamictization. Background noise intensity of the altered zircon is significantly higher than that of the unaltered material. High Raman background noise has been observed previously for trace-element-rich zircons and has been attributed to rare-earth-element-induced fluorescence (Wopenka et al., 1996). Trace-element analyses carried out on the study samples using the SHRIMP II indicate that dark, altered patches have consistently light heavy rare-earth-element (REE) concentrations than corresponding bright patches on the same grain (Sanborn, 2000). These results are consistent with the observations of Wopenka et al. (1996) and support a similar origin for the high background noise of altered domains of sample BNB-95-110c zircons.

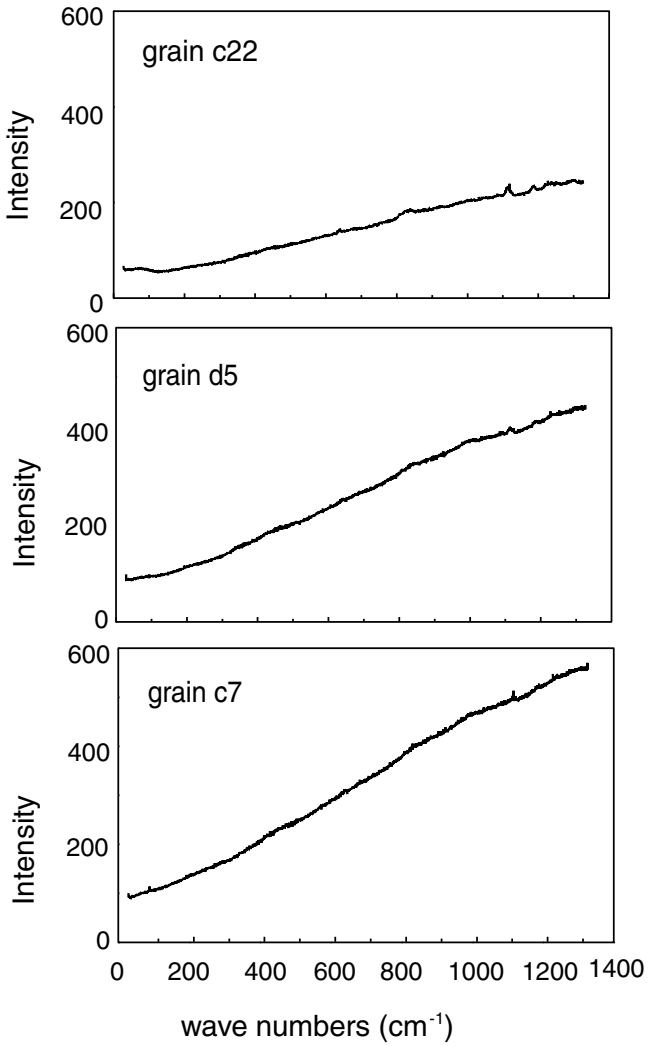

Figure 6. b) *Raman spectra of the altered domains (dark in back-scattered electron images) of three typical zircons from sample 110c. There is no indication of the SiO_4 stretching peak at roughly 1000 cm^{-1}, which suggests that the analyzed parts of the zircons are completely metamict. The higher background for the altered zircon is accounted for by increased rare-earth-element fluorescence.*

Table 3. Radiation dose for sample BNB-95-110c

Sample	Feature in back-scattered electron image	Radiation dose (alpha-event/mg)
82.1-D23.1*	bright	2.1×10^{16}
82.2-A4.1	bright	1.3×10^{16}
82.1-E8.1	dark	3.6×10^{16}
28.2NM1-14.3	dark	6.2×10^{16}
*grain used in TEM analysis		

Uranium and thorium concentrations used in the radiation dose calculation for sample BNB-95-110c were obtained from SHRIMP analyses of specific unaltered and altered spots. An age of 2.87 Ga was assumed in the radiation dose calculations presented in Table 3. In all cases the total accumulated doses exceed the threshold needed to reach amorphization according to Murakami et al. (1991).

Transmission electron microscopy results

Bright-field diffraction contrast images and selected-area diffraction patterns were collected from TEM membranes from two separate zircon grains. The brightness in the diffraction-contrast images is controlled by the degree to which an area diffracts incoming electrons. In bright-field images, increased brightness is due to the poor diffraction properties of damaged or noncrystalline material (i.e. brighter = more metamict). The diffraction patterns offer another qualitative means of determining the crystallinity of a very small area, with a diameter on the order of 200 nm limited by a selected-area aperature.

The membrane collected from grain d23 is composed of an unaltered zone, a very dark transition zone, and an adjacent altered patch, as observed in back-scattered electron imaging. A bright-field image of the entire membrane is given in Figure 7a. The membrane can be divided into three sections by the intersection of three linear features. It is oriented such that the darker, irregular, speckled part in the top left half of the image corresponds to the unaltered patch observed in the back-scattered electron image. Selected-area diffraction patterns were collected along a transect on both sides of the linear feature in the lower left side of the membrane. The pattern collected in the zone believed to be the unaltered zircon displays diffuse elliptical diffraction spots as shown, for example, in Figure 7c, spot 1. This type of pattern is consistent with a distorted, but crystalline, lattice. The mottled appearance of the unaltered zircon in the bright-field image is interpreted to be due to 3 to 5 nm microcrystals that are off axis by less than 1° with respect to their neighbours. The absence of halos in this diffraction pattern suggests a negligible component of amorphous material in the unaltered zircon.

Selected-area diffraction patterns collected from both sides of the lower left boundary show that each is composed of diffuse, but distinct, diffraction spots, although the

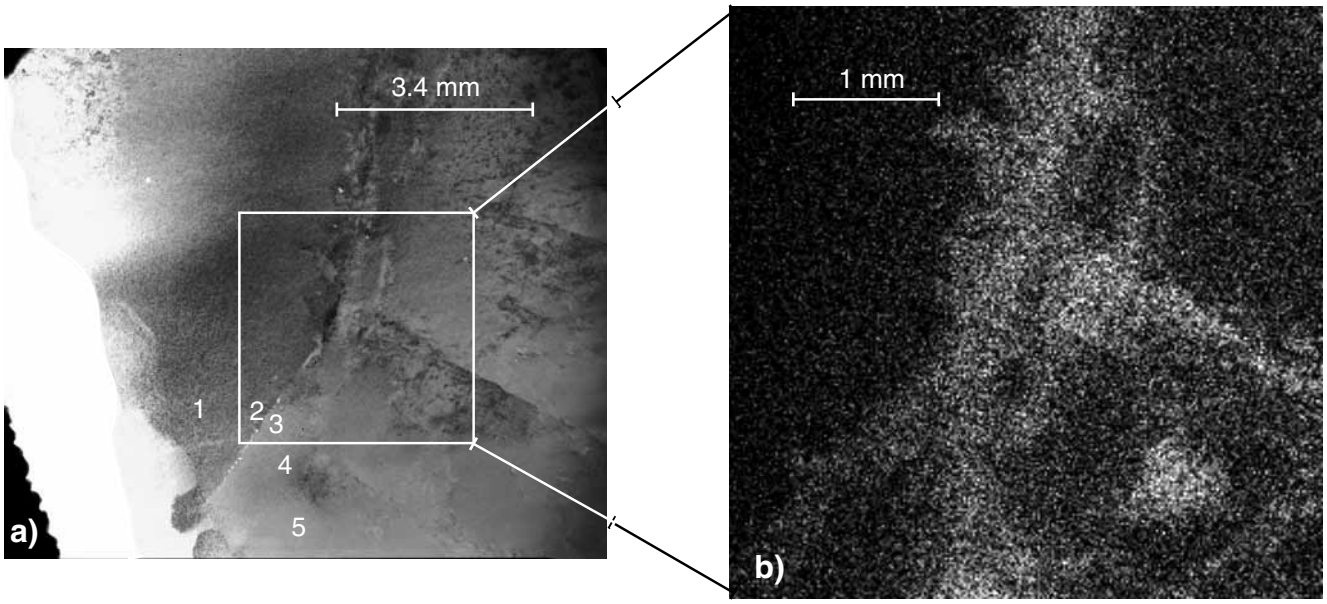

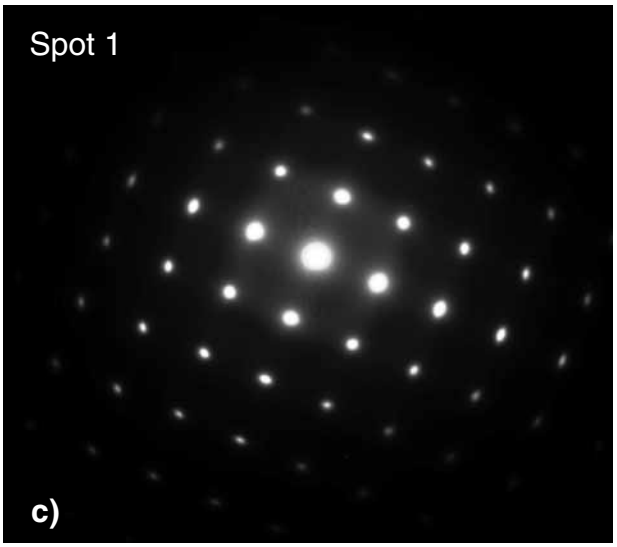

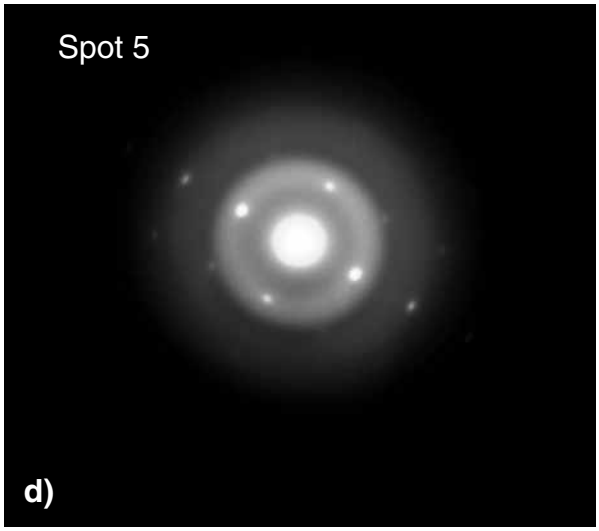

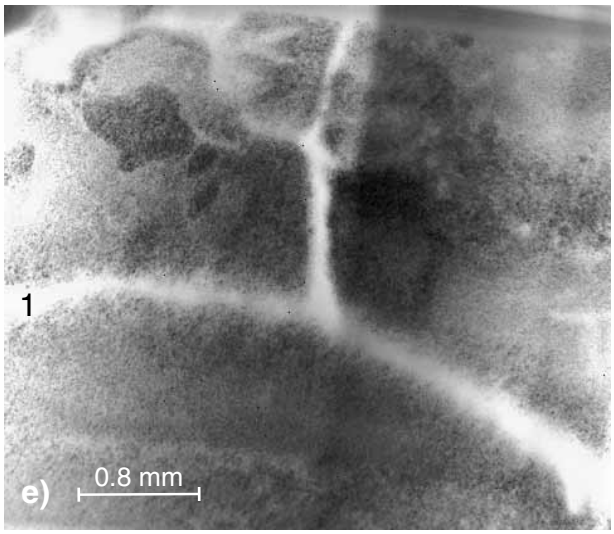

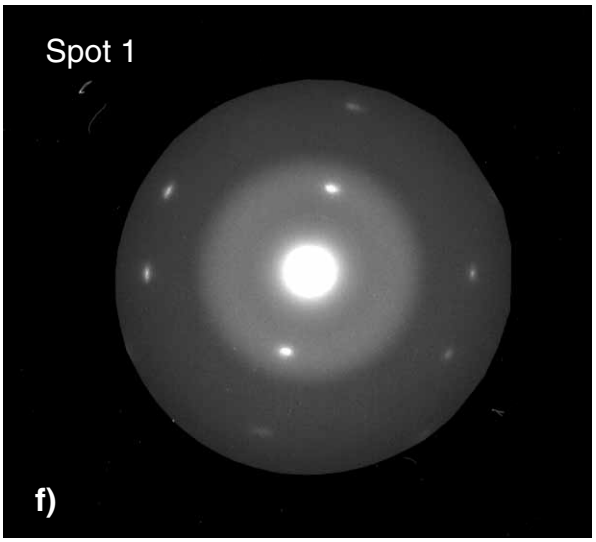

Contents/Contenu
Page 1 report/Début de l'article

distribution of spots around the central beam varied for each analysis (Fig. 7a, spots 2 and 3, selected-area diffraction patterns not shown). This suggests that the sharp linear feature is in fact a grain boundary between two crystalline domains of zircon that are slightly off axis with respect to each other. The bright, rectilinear features along the junction are tiny holes, likely the result of the accumulation of defects.

Other selected-area diffraction patterns were collected farther below the lower left grain boundary. The diffraction pattern from spot 4 (not shown) contains both weak diffraction spots and diffuse halos, indicating a mixture of crystalline and amorphous material. Farther from the boundary, the diffraction pattern is dominated by diffuse halos, suggesting a complete loss of crystallinity (Fig. 7d, spot 5). These data suggest that the transition from crystalline to amorphous zircon is progressive. The diffraction behaviour, illustrated by the brightness in the bright-field image, also changes gradually from a dark, speckled appearance for the unaltered zircon to a brighter, more homogeneous appearance for the altered zircon.

Energy-dispersive maps of a number of elements (Si, Zr, U, Pb, Ca, O, Ga), counted for five hours, were collected from the membrane. Calcium is the only element to show any detectable heterogeneity (Fig. 7b). As expected from previous electron probe analyses, the unaltered (top left) area of the membrane has no detectable Ca (Sanborn, 2000). The selected-area diffraction pattern from spot 1 was collected from this low-Ca domain. The sharp lower left boundary, believed to be a grain boundary and not a sharp transition to amorphous zircon, corresponds to only a moderate increase in Ca. Spot 4 within this moderate-Ca zone has a mixed diffraction pattern. A more significant increase in Ca occurs in the lower central part of the energy-dispersive map. Although the amorphous domain (Fig. 7d, spot 5) is not within the field sampled by the energy-dispersive map, examination of the bright -field image (Fig. 7a) suggests that spot 5 is in the zone characterized by high-Ca content.

A gradual transition to increasing Ca contents appears to be correlated with a gradual transition to a more amorphous structure (Fig. 8). Prior electron microprobe analysis analyses (Sanborn, 2000) suggest that the darkest zones in back-scattered electron images have the highest Ca content, on the order of 2% by weight. The boundary between bright and dark zircon in this membrane is defined by an exceptionally dark rim. Therefore, the area of highest Ca content in the energy-dispersive map (Fig. 7b) is interpreted to correspond to the transition to altered zircon observed in the back-scattered electron image. The other two branches of the triple junction (upper and lower right; Fig. 7d) are diffuse and defined by an increase in Ca content. Although the boundary between altered and unaltered zircon is very sharp in back-scattered electron images, the same boundary appears less distinct in the energy-dispersive map and bright-field image because of the smaller sampling scale of these images.

Another membrane was milled entirely from an altered patch of grain TEM11. A bright-field image of part of the membrane is shown in Figure 7e. Most of the membrane consists of speckled patches of variable brightness. The selected-area diffraction pattern from these patches is composed of distinct spots, again indicating a distorted, microcrystalline structure. Energy-dispersive maps indicate lesser Ca content in these regions. The most prominent feature observed in the bright-field image of this membrane is a very bright, T-shaped vein. Energy-dispersive maps show an even wider band of high-Ca material centred on the vein, but extending into the surrounding zircon. Selected-area

Figure 7.

TEM results for sample BNB-95-110c. See text for complete description of results. ***a)*** *Bright-field image of zircon membrane from grain d23. Metamict areas appear bright. The dashed line represents the top of the membrane. The bright white area to the left of the dashed line is empty space. The rectangle outlines the boundary of the energy-dispersive map. Numbers 1 to 5 represent the location of selected-area diffraction pattern analyses.* ***b)*** *Energy-dispersive map of Ca for part of the membrane. Note the enrichment of Ca in the centre and lower right of the map.* ***c)*** *Diffraction pattern from spot 1, illustrating a distorted, but crystalline, structure in the unaltered zircon.* ***d)*** *Diffraction pattern for spot 5, illustrating a metamict structure.* ***e)*** *Bright-field image of grain 11 showing a prominent, bright (metamict) vein and the location of the selected-area diffraction analysis.* ***f)*** *Diffraction pattern from the bright vein. The sharp boundary between the background and the diffraction pattern is the result of an aperature inserted to reduce charging effects.*

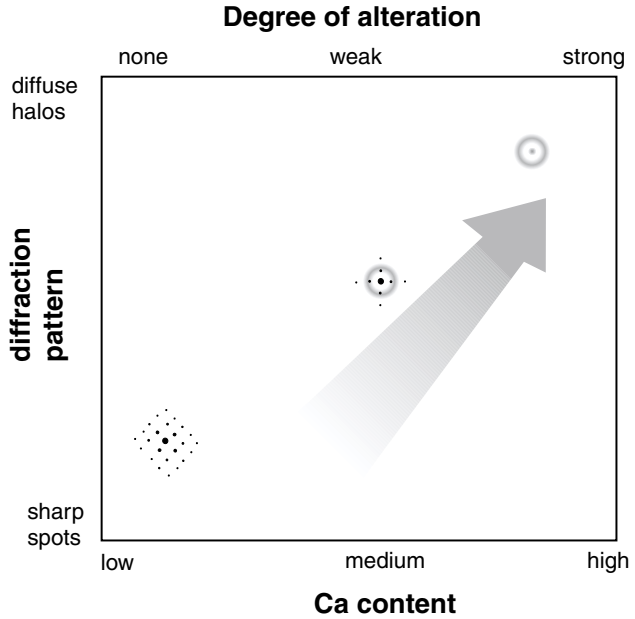

Figure 8. *Schematic diagram of the transition from unaltered to altered zircon. See text for discussion.*

diffraction patterns from the bright vein are composed of diffuse halos, indicating a total loss of short-range order (Fig. 7f). At the scale of the TEM analyses, altered zircon (a dark patch in the back-scattered electron images) appears to be composed of domains of high-Ca, amorphous material and lower Ca, partly crystalline material.

In summary, both zircon membranes contain amorphous domains that are highly enriched in Ca. Similar results are reported by Kurz and Hansen (1999). There are no signs of other crystalline phases in the diffraction patterns of the high-Ca zircon, and energy-dispersive spectra do not indicate other elements, such as P, in sufficient abundance to account for the Ca as an intergrowth of another discrete mineral phase, such as apatite. Therefore we conclude that the Ca in the zircon structure is found as interstitial atoms in the distorted crystal lattice.

DISCUSSION

The transition of zircon to a largely glassy state, such as that achieved by complete metamictization, is the simplest interpretation for the absence of Raman peaks in both altered and unaltered domains of Acasta granite zircons described here. Total metamictization is also predicted by the calculated radiation dose for both types of zircon, which greatly exceeds the thresholds for amorphization proposed by X-ray diffraction, infrared, and TEM studies (Holland and Gottfried, 1955; Chakoumakos et al., 1987; Murakami et al., 1991; Woodhead et al., 1991).

The Raman data, however, are not consistent with the TEM observations of the unaltered zircon, the latter indicating the presence of crystallinity. Clearly the differences between these measures of crystal structure must be reconciled. The TEM diffraction patterns convincingly demonstrate the crystallinity of the unaltered zircon. The observed crystallinity is inherent and could not have been induced during membrane milling, as only a transition to an amorphous structure has been attributed to interactions with the focused Ga^+ ion beam. Amorphization occurs mainly in extreme cases of very thin samples (20–30 nm) and in implantation rather than polishing, as was done in our work.

The absence of the Raman signal from such unaltered, microcrystalline zircon is curious and requires explanation. The defects associated with the boundaries between the slightly misaligned microcrystals constituting the unaltered zircon should result in broadened and weakened Raman signals. However, photoluminescence from impurities such as U, REE, or mineral inclusions will increase the background noise, and could overwhelm an already weak Raman signal. The area sampled by the Raman beam is roughly 20 μm wide by 100 μm deep. This poor control on the depth of analysis means that some interference is likely from any altered zircon underlying the unaltered domains. The most likely result of interaction with altered zircon would be increased photoluminescence due to Ca and REE enrichment. Additional systematic experiments are needed to constrain the effect of the microcrystalline structure and to confirm that the loss of Raman peaks is due to a signal-to-noise ratio below the sensitivity of the instrument. The Raman sampling volume appears to be much larger than the internal features observed in back-scattered electron imaging. As both altered and unaltered zircon have likely been sampled in a single analysis, the Raman data may be considered a measure of the bulk structure of the grain. The X-ray diffraction pattern from a single zircon grain from sample BNB-95-110c shows a largely amorphous structure, also consistent with the absence of Raman peaks (R. Stern, unpub. data, 1999).

Although the Raman data can be reconciled with the electron diffraction patterns, we are still left with radiation dose calculations well above the thresholds for complete metamictization. The diffuse elliptical diffraction spots from low-Ca zircon in both unaltered and weakly altered domains correspond to a distorted, but not amorphous, structure (Fig. 7c). The bright-field imaging data are consistent with a structure composed of a mosaic of misaligned, 3 to 5 nm microcrystals. The diffraction patterns observed are similar to the diffraction patterns linked by Chakoumakos et al. (1987) and Murakami et al. (1991) to a radiation dose of 0.3 x 10^{16} to 0.8 x 10^{16} alpha-events/mg, an intermediate crystal state. However, the radiation dose calculated using the age and U content of grain d23 is 2.1 x 10^{16} alpha-events/mg, well above the threshold for metamictization. At this dose, a diffraction pattern composed of diffuse halos would be expected (Holland and Gottfried, 1955; Chakoumakos et al., 1987; Murakami et al., 1991; Woodhead et al., 1991).

A mechanism is needed to account for the discrepancy between the dose calculations, which are consistent with complete metamictization, and the TEM diffraction patterns, which reveal a distorted, but crystalline, structure. One of the samples characterized by Nasdala et al. (1998) has U and Th concentrations and ages comparable to those of sample BNB-95-110c. In that study, zircon from Jack Hills, Australia, is composed of zoned and unzoned zircon, and both types meet or exceed the radiation dose required for metamictization (Nasdala et al., 1998). However, the unzoned zircon still preserves a narrow Raman peak consistent with intermediate crystallinity and yields concordant age data. Nasdala et al. (1998) account for the difference between Raman peak width and radiation dose by invoking inhomogeneous recrystallization later in the geological history of the sample. A similar recrystallization mechanism is proposed here for sample BNB-95-110c. The crystallinity observed in the study sample corresponds to a dose of roughly 0.3 x 10^{16} to 0.4 x 10^{16} alpha-events/mg. To have accumulated this minor amount of damage, recrystallization must have occurred a considerable time after primary growth. Assuming average U and Th concentrations of 1000 ppm and 100 ppm respectively, complete recrystallization at ~1000 Ma would result in a dose of 0.4 x 10^{16} alpha-events/mg, comparable to the observed diffraction pattern. Very large errors are associated with this calculation due to uncertainty in the U and Th concentration used and in the actual dose represented by the diffraction pattern from sample BNB-95-110c. However, this calculation is intended simply to give a first-order reference to the earliest time of recrystallization. If recrystallization did occur, the process did not exclude Pb from the new structure, as concordancy is

maintained in the newly crystalline zircon. Recrystallization without accompanying Pb loss was also assumed for the Jack Hills zircon mentioned above (Nasdala et al., 1998). However, in many cases recrystallization is thought to be a important mechanism driving Pb loss and discordance (Pidgeon, 1992; Mezger and Krogstad, 1997).

CONCLUSIONS

A comparison of Raman spectroscopic spectra, TEM diffraction patterns, and calculated radiation doses has allowed us to characterize the microstructure of zircon from a high-U, late Archean rock. SHRIMP isotopic data (Sanborn, 2000) suggest that alteration is responsible for Pb loss in this sample, and the microstructure data presented here shed some light on the alteration mechanism. The following points summarize the key observations of this study:

1. Unaltered zircon, which appears bright in back-scattered electron images, is interpreted to be composed of a mosaic of slightly misaligned microcrystals and contains a negligible amorphous component.
2. Altered zircon, which appears dark in back-scattered electron images, has a heterogeneous microstructure composed of domains of both distorted crystalline and amorphous zircon.
3. Low-Ca domains have been subject to recrystallization late in the geological history of this sample, and Pb loss did not accompany recrystallization.
4. A qualitative correlation exists between the amount of Ca in the structure and the extent of the amorphous structure.
5. The Ca is restricted to discrete veins or patches. There is no indication of secondary, Ca-rich phases. We conclude that the Ca is present as lattice impurities.

Although more study is required, we can suggest a tentative order for the various processes of metamictization, alteration, and recrystallization. Uranothorite inclusions, ranging in size from 1 to 50 μm, are disseminated throughout the altered domains of sample BNB-95-110c zircons. SHRIMP U-Pb analysis of these inclusions suggests that alteration and the concomitant addition of Ca along discrete veins occurred ca. 2200 Ma (N. Sanborn and R. Stern, unpub. data, 1999). By this time, the primary, 2875 Ma zircon was already significantly damaged, having accumulated between 0.25×10^{16} and 1.8×10^{16} alpha-events/mg, depending on local U content. These pre-existing defects were sufficient to accommodate large Ca ions introduced by fluids at 2200 Ma. From first-order calculations, significant recrystallization is unlikely to have occurred before 1000 Ma or before the introduction of the Ca cations. Recrystallization took place in low-Ca regions in both bright and dark patches. Extreme distortion in the high-Ca domains may have prohibited the reorganization of the lattice into a zircon structure during recrystallization. Regardless of the exact timing, recrystallization is unlikely to have occurred before input of Ca, as it would be very difficult to accommodate large Ca cations into the crystalline zircon structure.

Although recrystallization appears to be the only feasible explanation for the crystalline nature of these Archean zircons, little work has been done on the characterization of the microstructure of zircon as ancient as that in Acasta sample BNB-95-110c. To date, most TEM studies concerned with the metamict structure of natural zircon have examined the ca. 570 Ma or younger Sri Lankan zircon megacrysts. Further study into the microstructure of Archean zircon may reveal patterns or behaviour, such as recrystallization unaccompanied by Pb loss, not observed in younger zircon.

ACKNOWLEDGMENTS

The results presented in this paper form part of the senior author's M.Sc. thesis; N.S. wishes to acknowledge the financial support of a Natural Sciences and Engineering Research Council of Canada (NSERC) postgraduate scholarship and an NSERC research grant to S. Carr (Carleton University, Ottawa). Thanks go to W. Bleeker for providing the rock sample. Rob Patterson is thanked for his expertise in preparing zircon membranes for TEM analysis. The manuscript benefited from critical reviews by M. Hamilton and S. Carr.

REFERENCES

Black, L.P. and Gulson, B.L.
1978: The age of the Mud Tank carbonatite, Strangeways Range, Northern Territory; Bureau of Mineral Resources, Journal of Australian Geology and Geophysics, v. 3, p. 227–232.

Bowring, S.A., Williams, I.S., and Meyer, C.
1989: 3.96 Ga gneisses from the Slave Province, Northwest Territories, Canada; Geology, v. 17, p. 971–975.

Bursill, L.A. and McLaren, A.C.
1966: Transmission electron microscope study of natural radiation damage in zircon ($ZrSiO_4$); Physica Status Solidi, v. 13, p. 331–343.

Chakoumakos, B.C., Murakami, T., Lumpkin, G.R., and Ewing, R.C.
1987: Alpha-decay-induced fracturing in zircon: the transition from the crystalline to the metamict state; Science, v. 236, p. 1556–1559.

Desgreniers, S. and Lagarec, K.
1994: XRDA: A program for energy-dispersive X-ray diffraction analysis on a PC; Journal of Applied Crystallography, v. 27, p. 432–434.

Farges, F. and Calas, G.
1991: Structural analysis of radiation damage in zircon and thorite: an X-ray absorption spectroscopic study; American Mineralogist, v. 76, p. 60–73.

Holland, H.D. and Gottfried, D.
1955: The effect of nuclear radiation on the structure of zircon; Acta Crystallographica, v. 8, p. 291–300.

Irmer, G.
1985: Zum Einfluß der Apparatefunktion auf die Bestimmung von Streuquerschnitten und Lebensdauern aus optischen Phononenspektren; Experimentelle Technik der Physik, v. 33, p. 501–506.

Kurz, S. and Hansen, B.T.
1999: The influence of hydrothermal alteration on the U/Pb system of zircons — EMS and TIMS studies; Terra Abstracts, v. 11, p. 800.

Mezger, K., and Krogstad, E.J.
1997: Interpretation of discordant U-Pb zircon ages: an evaluation; Journal of Metamorphic Geology, v. 15, p. 127–144.

Mortensen, J.K.
1993: U-Pb geochronology of the eastern Abitibi Subprovince. Part 2: Noranda–Kirkland Lake area; Canadian Journal of Earth Sciences, v. 30, p. 29–41.

Murakami, T., Chakoumakos, B.C., Ewing, R.C., Lumpkin, G.R., and Weber, W.J.
1991: Alpha-decay event damage in zircon; American Mineralogist, v. 76, p. 1510–1532.

Nasdala, L., Irmer, G., and Wolf, D.
1995: The degree of metamictization in zircon: a Raman spectroscopic study; European Journal of Mineralogy, v. 7, p. 471–478.

Nasdala, L., Pidgeon, R.T., and Wolf, D.
1996: Heterogeneous metamictization of zircon on a microscale; Geochimica et Cosmochimica Acta, v. 60, p. 1091–1097.

Nasdala, L., Pidgeon, R.T., Wolf, D., and Irmer, G.
1998: Metamictization and U-Pb discordance in single zircons: a combined Raman microprobe and SHRIMP ion probe study; Mineralogy and Petrology, v. 62, p. 1–27.

Pidgeon, R.T.
1992: Recrystallization of oscillatory zoned zircon: some geochronological and petrological implications; Contributions to Mineralogy and Petrology, v. 110, p. 463–472.

Roberts, S., and Beattie, I.
1995: Micro-Raman spectroscopy in the Earth Sciences; *in* Microprobe Techniques in the Earth Sciences, (ed.) P.J. Potts, J.F.W. Bowles, S.J.B. Reed, and M.R. Cave; Chapman and Hall, London, England, p. 387–408.

Sanborn, N.
2000: Microprobe studies of alteration, discordance and metamictization in late Archean zircons from the Acasta Gneiss Complex, Canada; M.Sc. thesis, Carleton University, Ottawa, Ontario, 178 p.

Silver, L.T., and Deutsch, S.
1963: Uranium-lead isotopic variations in zircons: a case study; Journal of Geology, v. 71, p. 721–758.

Stern, R.A.
1997: The GSC Sensitive High Resolution Ion Microprobe (SHRIMP): analytical techniques of zircon U-Th-Pb age determinations and performance evaluation; *in* Radiogenic Age and Isotopic Studies: Report 10; Geological Survey of Canada, Current Research 1997-F, p. 1–31.

Stern, R.A. and Bleeker, W.
1998: Age of the world's oldest rocks refined using Canada's SHRIMP: the Acasta Gneiss Complex, Northwest Territories, Canada; Geoscience Canada, v. 25, p. 27–31.

Wasilewski, P.J., Senftle, F.E., and Vaz, J.E.
1973: A study of the natural alpha-recoil damage in zircon by infrared spectra; Radiation Effects, v. 17, p. 191–199.

Woodhead, J.A., Rossman, G.R., and Silver, L.T.
1991: The metamictization of zircon: radiation dose-dependent structural characteristics; American Mineralogist, v. 76, p. 74–82.

Wopenka, B., Jolliff, B.L., Zinner, E., and Kremser, D.T.
1996: Trace element zoning and incipient metamictization in a lunar zircon: application of three microprobe techniques; American Mineralogist, v. 81, p. 902–912.